Plasmonic analogue of electromagnetically induced transparency at the Drude damping limit

Na Liu[1], Lutz Langguth[1], Thomas Weiss[1], Jürgen Kästel[2], Michael Fleischhauer[2], Tilman Pfau[3] and Harald Giessen[1]*

In atomic physics, the coherent coupling of a broad and a narrow resonance leads to quantum interference and provides the general recipe for electromagnetically induced transparency (EIT). A sharp resonance of nearly perfect transmission can arise within a broad absorption profile. These features show remarkable potential for slow light, novel sensors and low-loss metamaterials. In nanophotonics, plasmonic structures enable large field strengths within small mode volumes. Therefore, combining EIT with nanoplasmonics would pave the way towards ultracompact sensors with extremely high sensitivity. Here, we experimentally demonstrate a nanoplasmonic analogue of EIT using a stacked optical metamaterial. A dipole antenna with a large radiatively broadened linewidth is coupled to an underlying quadrupole antenna, of which the narrow linewidth is solely limited by the fundamental non-radiative Drude damping. In accordance with EIT theory, we achieve a very narrow transparency window with high modulation depth owing to nearly complete suppression of radiative losses.

Electromagnetically induced transparency (EIT) is a quantum interference effect that reduces light absorption over a narrow spectral region in a coherently driven atomic system[1–3]. Associated with the enhanced transmission is a drastic modification of the dispersive properties of the medium, which enables light to be slowed down substantially[4–7]. Recently, a lot of attention has been paid to the fact that EIT-like effects can occur in classical oscillator systems. Examples include coupled microresonators[8], electric circuits[9], a waveguide side-coupled to resonators[10,11] and metallic structures[12]. In particular, the theoretical prediction of plasmon-induced transparency has been brought forward[13]. However, so far experimental attempts to realize these theoretical proposals in optical plasmonic systems have not been successful owing to difficulties associated with nanofabrication. Very recently, Fano resonances within an absorption band have been experimentally observed in non-optimized single plasmonic structures at optical frequencies[14]. The broad linewidth and small modulation depth of those resonances, however, severely hamper applications such as slowing down light, which requires an abrupt change in dispersion over a narrow spectral range, as well as sensing, where a sharp and pronounced spectral response is highly desired[15].

Here, we provide the first experimental demonstration of EIT-like effects in optical metamaterials. The structure of this nanoplasmonic analogue of EIT consists of two functional layers, where each unit cell comprises a gold bar stacked above two symmetric gold wires (Fig. 1a). The elements in the two layers are oriented perpendicular to each other. More specifically, the top gold bar serves as a broad-linewidth dipole antenna. It is strongly coupled to light, therefore suffering significant losses due to radiative damping. The bottom gold wire pair can act as a non-radiative quadrupole antenna and its resonance frequency is adjusted within the absorbance profile of the dipole antenna. The damping of the quadrupole antenna stems almost exclusively from intrinsic metal losses (Drude damping), and is much smaller than the radiative damping of the dipole antenna. Owing to

close proximity, the two antennas can be strongly coupled. As a consequence, destructive interference between the two excitation pathways leads to the EIT-like phenomena. These two pathways are the direct excitation of the dipole antenna by the external light field and the excitation by the coupling with the quadrupole antenna. On the contrary, if the underlying quadrupole antenna is replaced by a dipole antenna, which has similar damping to the upper one, the destructive interference disappears and no enhanced transmission effect can be observed. This is the distinctive signature of normal-mode splitting in contrast to EIT behaviour. In addition, we experimentally demonstrate that the EIT-like spectra can be modified by varying the coupling strength between the dipole and quadrupole antennas by means of accurate structural tuning. The agreement between experiment and a simple EIT model[3,9] is nearly perfect. Moreover, we demonstrate that our experimental absorbance linewidth is limited only by Drude damping. The resulting narrow, yet fully modulated EIT-like features, render our nanoplasmonic system ideal for slow light and novel sensors with high sensitivity[16].

Figure 1a schematically shows the metamaterial structure. The upper gold bar (in red) is stacked above the underlying gold wire pair (in green) with a vertical distance $h = 70\,\text{nm}$. The lateral displacement of the bar with respect to the symmetry axis of the wire pair is defined as s. Electron micrographs of the samples fabricated by nanofabrication stacking techniques[17] were obtained by field-emission scanning electron microscopy. Figure 1b shows an oblique incidence overview of a typical sample with a lateral displacement $s = 10\,\text{nm}$. An enlarged oblique view is given in the inset of Fig. 1b, demonstrating excellent alignment accuracy between the two functional layers. The optical properties of the samples at normal incidence were measured with a Fourier-transform infrared spectrometer with electric field polarization along the dipole antenna. In the following, we are going to show systematic tuning of the EIT-like spectra in these stacked samples by introducing structural asymmetry. The experimental transmittance (green
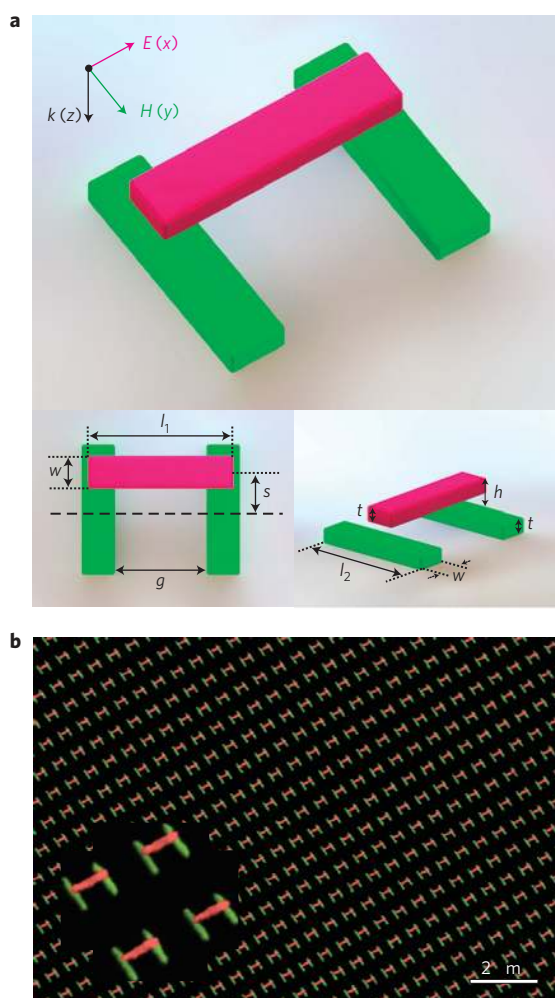

1

Figure 1 | Structural geometry and field-emission electron microscopy images. a, Schematic diagram of the stacked plasmonic EIT structure with definitions of the geometrical parameters: $l_1 = 355$ nm, $l_2 = 315$ nm, $w = 80$ nm, $g = 220$ nm, $t = 40$ nm and $h = 70$ nm. The periods in both the x and y directions are 700 nm. Red colour represents the gold bar in the top layer and green colour represents the gold wire pair in the bottom layer. **b**, Oblique view of the sample with lateral displacement $s = 10$ nm. Inset: Enlarged view. All of the structures were fabricated on a glass substrate. The gold wires were embedded in a photopolymer (PC403), which serves as a dielectric spacer.

circles), reflectance (pink circles) and absorbance spectra (black circles) in dependence on the lateral displacement s are presented in Fig. 2. The absorbance spectra were calculated using $A = 1 - T - R$. In the absence of structural asymmetry, that is, for $s = 0$, there is only a single resonance ($\omega_0 = 170$ THz) observable in the absorbance spectrum (see Fig. 2b). The origin of this resonance is attributed to the excitation of dipole-like plasmons inside the upper gold bar. This gold bar works as a dipole antenna and radiates strongly to free space, giving rise to a broad resonance in the spectrum. The lower wires do not contribute, as the elements in the two layers are not coupled to each other in the absence of symmetry breaking.

The coupling between the two layers starts once the structural asymmetry is introduced. As visible in the case of $s = 10$ nm, a transmittance peak in Fig. 2a (an absorbance dip in Fig. 2b) at around 173 THz emerges near the centre of the broad resonance. A detuning parameter δ is introduced to define the frequency difference between the quadrupole and dipole resonances. In our case, δ is approximately 3 THz, resulting from slightly too short

bottom wires owing to the fabrication process. By further enlarging the lateral displacement s, the coupling strength between the dipole and quadrupole antennas is successively increased. As a result, the transparency window at 173 THz grows in strength and becomes more and more prominent as shown in Fig. 2a. We interpret the above phenomena in terms of plasmonic EIT. Particularly, the narrow linewidths and high modulation depths of these EIT-like features indicate the drastically low loss in the quadrupole antenna. The physics of the plasmonic EIT can be better understood if we examine the analogy between our system and atomic EIT systems[3,13]. Figure 3a shows a prototype three-level system for EIT, in which $|0\rangle$ is the ground state and $|1\rangle$ and $|2\rangle$ are the two upper states. $|0\rangle - |1\rangle$ defines a dipole-allowed transition, which is in analogy to the mode excited in the dipole antenna in our system. It is related to a photon frequency ω_0 and a dissipation rate γ_1. This rate includes two contributions, namely, radiative damping due to the transformation of particle plasmons into photons and non-radiative damping due to the intrinsic metal loss. $|0\rangle - |2\rangle$ defines a dipole-forbidden transition, which is in analogy to the mode that can be excited in the quadrupole antenna when structural asymmetry is present. It is characterized by a dissipation rate γ_2, which is mainly limited by the intrinsic metal loss. δ denotes the detuning from the transition line centre with the condition $\delta \ll \gamma_1$. The two damping factors satisfy $\gamma_2 \ll \gamma_1 \ll \omega_0$. The transition rate, κ, between states $|1\rangle$ and $|2\rangle$ is correlated with the coupling between the dipole and quadrupole antennas. Consequently, the two possible pathways, namely, $|0\rangle - |1\rangle$ and $|0\rangle - |1\rangle - |2\rangle - |1\rangle$ interfere destructively, therefore dramatically reducing losses and enhancing transmittance.

To further explore the EIT-like spectral characteristics, optical spectra and the electric field distribution are calculated on the basis of a scattering matrix algorithm[18] and on commercial finite-integration time-domain software. For bulk gold, the permittivity in the infrared spectral regime is described by the Drude model[19,20] with the plasmon frequency $\omega_{pl} = 2\pi \times 2.175 \times 10^{15}$ s^{-1} and the damping constant $\omega_c = 2\pi \times 6.5 \times 10^{12}$ s^{-1}. Owing to the surface scattering and grain boundary effects in the thin film, in the calculations we use a damping constant that is three times[21,22] as large as that in bulk gold, that is, about 20 THz. The overall agreement between experimental and calculated spectra is very good (see Supplementary Information). The electric field distribution at the absorbance dip as indicated by the red triangle in the case of $s = 50$ nm (see Fig. 2b) is shown in Fig. 3b. At resonance, the two underlying wires are characterized by antisymmetric charge oscillations, which correspond to the excitation of the quadrupole mode. The destructive interference leads to a nearly zero electric field in the top bar. In other words, owing to nearly complete suppression of radiative damping, the linewidth of these EIT-like features is solely limited by non-radiative damping, that is, intrinsic Drude loss of the metal. This makes our plasmonic EIT structures particularly promising for biomedical and chemical sensing.

As a control experiment, we also fabricated a stacked sample with only a single wire, that is, another dipole antenna, in the bottom layer. We define the lateral displacement of the top wire with respect to the symmetry axis of the bottom wire as Ds. Similarly, in the absence of structural asymmetry, that is, $Ds = 0$, the top and bottom wires are uncoupled, giving rise to a single absorbance peak in the spectrum (not shown). When structural asymmetry is introduced, that is, $Ds = 90$ nm, the two dipole antennas can be coupled. Such dipole–dipole coupling between the two wires results in a spectral splitting owing to the hybridization of the resonances of the two individual wires[23]. It is worth mentioning that 90 nm was selected because lateral displacements below this value do not lead to observable spectral splitting in experiments. The difference between the EIT-like spectrum and the spectrum arising from hybridization of plasmonic modes is remarkable. This becomes evident when comparing the two corresponding spectra associated with the same
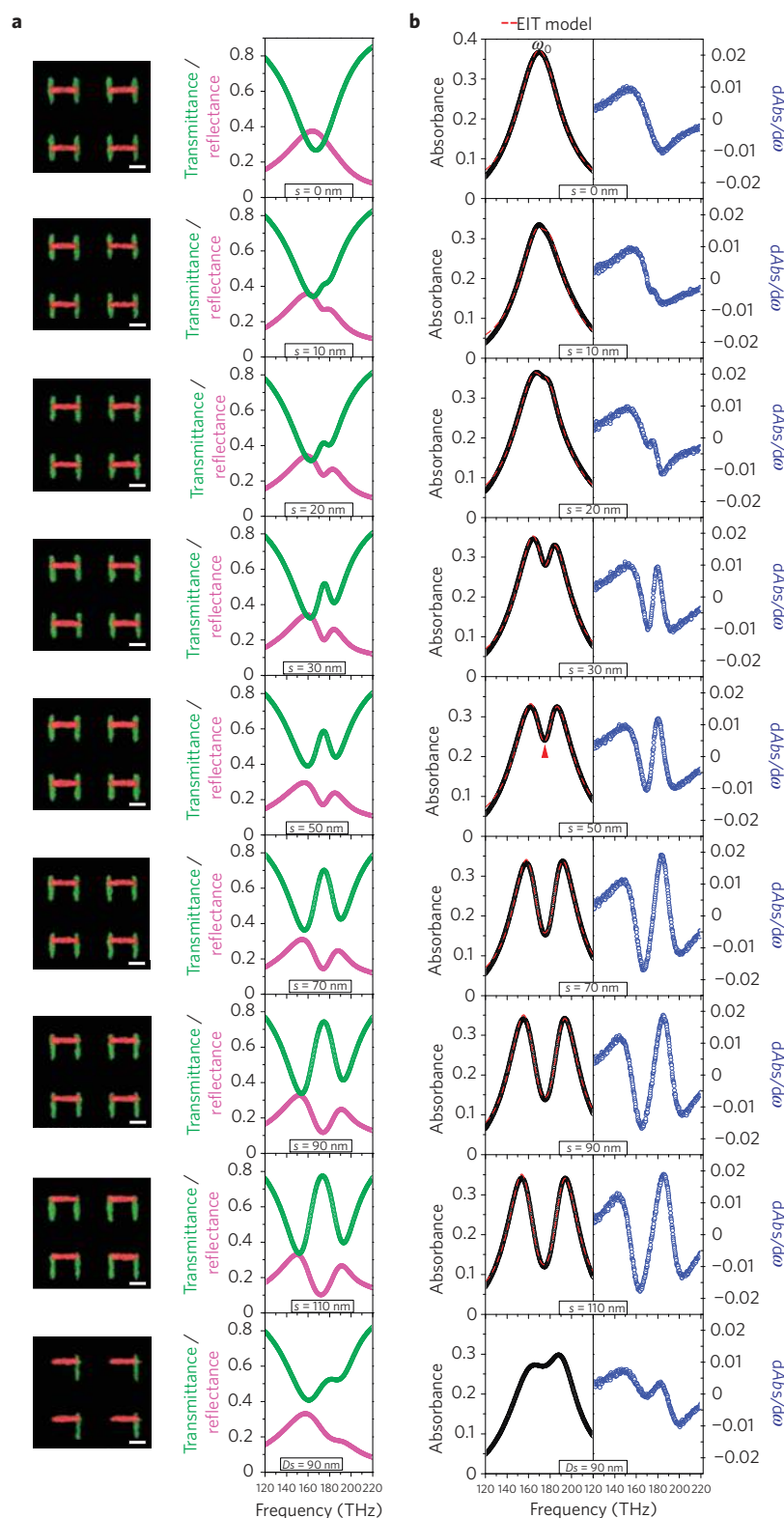
Figure 2 | Experimental transmittance, reflectance and absorbance spectra in dependence on lateral displacement. a, Scanning electron micrographs of the corresponding structures are shown in the left column. The scale bar is 200 nm. Green- and pink-circled curves represent the experimental transmittance and reflectance spectra, respectively. **b,** Black-circled curves represent the experimental absorbance spectra ($A = 1 - T - R$). Red-dashed lines represent the fitting curves calculated from the two-oscillator model. The blue-circled curves represent the derivatives dAbs/dω of the experimental absorbance spectra. The evolution of the EIT-like features in the absorbance spectra and their slopes show a strong dependence on the lateral displacement. The lowest spectrum shows the situation for two stacked dipole antennas, which are associated with normal-mode splitting rather than EIT. The remarkable difference between EIT-like behaviour and normal-mode splitting can be nicely distinguished when comparing the two cases of $s = 90$ nm (third lowest spectrum, dipole–quadrupole coupling) and $Ds = 90$ nm (lowest spectrum, dipole–dipole coupling) in the figure. The normal-mode splitting case shows only a slight dip in the absorbance spectrum.
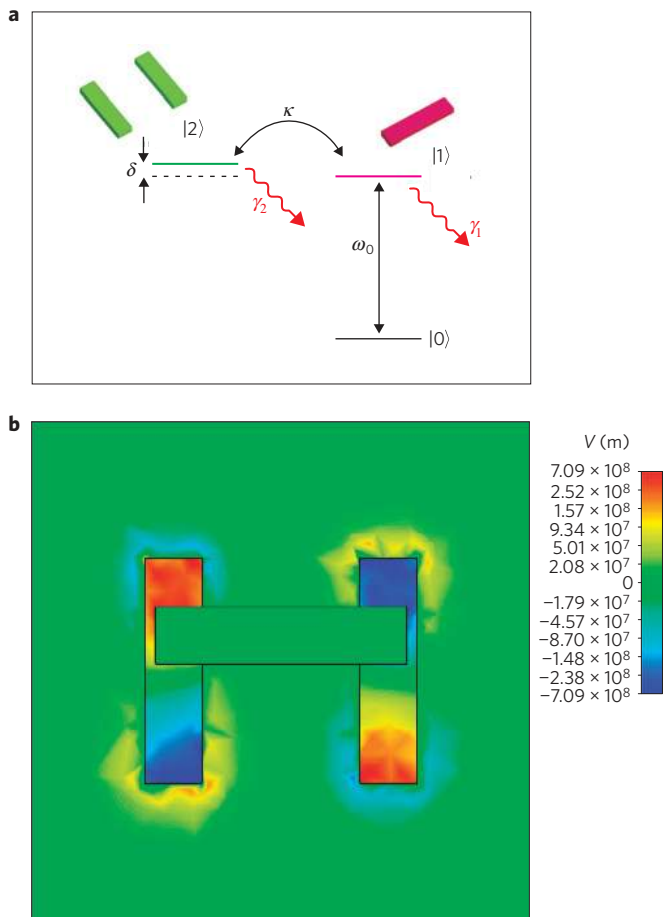
Figure 3 | Prototype system for plasmonic EIT and numerical electric field distribution. a, Level scheme for EIT in a prototype three-level system. δ denotes the detuning from the transition line centre. κ defines the transition rate between states $|1\rangle$ and $|2\rangle$. γ_1 includes non-radiative damping due to the intrinsic metal loss, and radiative damping due to the strong dipole characteristics. γ_2 contains only non-radiative (Drude) damping. The two possible pathways, namely, $|0\rangle$–$|1\rangle$ and $|0\rangle$–$|1\rangle$–$|2\rangle$–$|1\rangle$, interfere destructively and lead to the EIT-like phenomena. **b**, Electric field distribution at resonance as indicated by the red triangle for $s = 50$ nm in Fig. 2. Antisymmetric charge oscillations are excited in the bottom wire pair, whereas the top bar contains nearly no field.

lateral displacement, that is, $s = 90$ nm and $Ds = 90$ nm in Fig. 2b. More concretely, the EIT-like spectrum exhibits a prominently narrow and pronounced absorbance dip resulting from destructive interference. On the contrary, in the case of the normal-mode coupling, destructive interference is not expected owing to the fact that the two dipole antennas have similar dampings. The occurrence of the tiny absorbance dip in the spectrum is due to the overlap of the two hybridized resonance envelopes.

To evaluate our EIT-like spectra quantitatively, the derivatives dAbs/dω of the experimental absorbance spectra are plotted in Fig. 2b, which are characterized by blue-circled curves. The evolution of the slopes of the EIT-like features in dependence on the lateral displacement is apparently visible. Notably, the slopes of the EIT-like features are already steeper than those of the single plasmonic resonance ($s = 0$ nm) at $s = 50$ nm. Furthermore, as a maximum at $s = 90$ nm, a steepness ratio of 1.5 is achieved between the slopes of the EIT feature and plasmonic resonance. In contrast, for the dipole–dipole coupling case, the slopes of the absorbance dip are still flatter when compared with those of the single plasmonic resonance even at $s = 90$ nm.
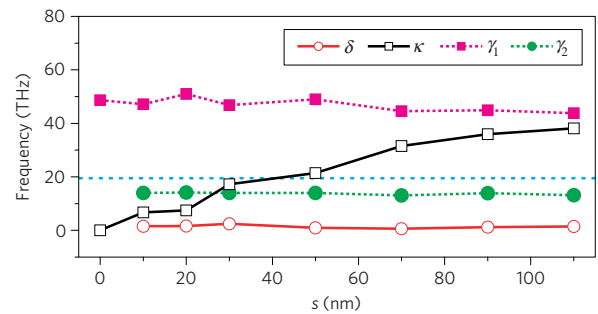

Figure 4 | Extracted experimental damping and coupling parameters as a function of lateral displacement s. Values of γ_1, γ_2, δ and κ extracted by fitting the experimental absorbance curves in Fig. 2b according to equation (3). The dashed-blue line represents the Drude damping limit of experimental thin gold films ($\sim$20 THz). Evidently, our extracted damping value of γ_2 is below this limit.

To provide a quantitative description of our plasmonic EIT system, we use a simple two-oscillator EIT model[3,13]. The dipole antenna in our structure is represented by oscillator 1, which is driven by an applied source $E(t)$. The quadrupole antenna is represented by oscillator 2, which can be excited only through coupling between the two oscillators. The charges $q_1(t)$ and $q_2(t)$ in oscillators 1 and 2 satisfy the coupled differential equations:

$$\ddot{q}_1(t) + \gamma_1\dot{q}_1(t) + \omega_0^2 q_1(t) + \kappa\dot{q}_2 = E(t) \tag{1}$$

$$\ddot{q}_2(t) + \gamma_2\dot{q}_2(t) + (\omega_0+\delta)^2 q_2(t) - \kappa\dot{q}_1 = 0 \tag{2}$$

Here ω_0 is the resonance frequency of oscillator 1 when it is isolated from oscillator 2. δ denotes the detuning of the resonance frequency of oscillator 2 from oscillator 1 ($\delta \ll \gamma_1$). γ_1 and γ_2 are the losses in oscillators 1 and 2, respectively ($\gamma_2 \ll \gamma_1 \ll \omega_0$). κ is the coefficient of the coupling between the two oscillators. After solving the equations (1) and (2) with the approximation $\omega - \omega_0 \ll \omega_0$ and therefore $\omega_0^2 - \omega^2 \approx -2\omega_0(\omega - \omega_0)$, the energy dissipation as a function of frequency is obtained as follows:

$$P(\omega) = \frac{i}{2}\frac{(\omega-\omega_0-\delta)+i\frac{\gamma_2}{2}}{\left(\omega-\omega_0+i\frac{\gamma_1}{2}\right)\left(\omega-\omega_0-\delta+i\frac{\gamma_2}{2}\right)-\frac{\kappa^2}{4}} \tag{3}$$

Subsequently, we fit the experimental absorbance spectra in Fig. 2b according to equation (3) and present the results by red-dashed curves in the same figure for a direct comparison. It is evident that the experimental curves are reproduced nearly perfectly by the fitted results. To examine the damping mechanism, Fig. 4 shows the fitting values for γ_1, γ_2, δ and κ as a function of lateral displacement s in frequency units. The detuning parameter δ is approximately 3 THz. The coupling coefficient κ is proportional to s and it increases successively with more structural asymmetry. γ_2 is roughly constant at 13 THz, which is nearly four times smaller than γ_1 ($\sim$50 THz). Such quantitative results substantiate our expectation on drastic reduction of losses in the quadrupole antenna due to nearly complete suppression of radiative coupling. It is noteworthy that the damping frequency correlated with the intrinsic loss in thin gold films in the near-infrared is about 20 THz (refs 21, 22) (see blue-dashed line in Fig. 4). Astonishingly, in our case γ_2 amounts to only 13 THz. This implies that the non-radiative damping in our system is also substantially reduced. The origin of this suppression of non-radiative damping becomes immediately apparent from the electric field distribution as shown in Fig. 3b. We found that at resonance, a significant amount of the electric field is outside the gold wires and dissipates in the dielectric environment[24],

which is the photopolymer PC403 (see the Methods section). Its dielectric losses are indeed negligible at optical frequencies. In essence, the damping in our plasmonic EIT system is below the Drude damping of thin gold films (20 THz) and even approaches the Drude damping limit of bulk gold (6.5 THz; refs 19, 20). Such drastic reduction of damping leads to the extremely narrow linewidth of the quadrupole mode and hence greatly facilitates the plasmonic EIT effects.

The concept of plasmonic EIT provides deep insight into achieving low-loss optical metamaterials for future applications. This arises from the fact that reducing losses is one of the main challenges in this field. In particular, the non-radiative damping could be further reduced by careful tailoring of the electric field inside and outside the quadrupole antenna. Another benefit afforded by our plasmonic EIT analogue is the ability to construct light-slowing devices[25,26]. The realization of dipole–quadrupole coupling holds great promise for designing and understanding complex plasmonic structures associated with higher-order multipolar interaction mechanisms[27]. Furthermore, the possibility of accurately tuning plasmonic response by using structural asymmetry makes our metamaterial structures particularly interesting as a model system for comprehending light–matter interaction phenomena. In addition, the narrow and fully modulated EIT-like features due to the extraordinary reduction of damping are exciting news for novel devices in the field of chemical and biomedical sensing.

Methods

Structure fabrication. Three (or more) gold alignment marks (size $4\,\mu m \times 100\,\mu m$) with a gold thickness of 250 nm are first fabricated by lift-off on a quartz substrate. The substrate is then covered with a 40 nm gold film using electron-beam evaporation. Next, wire-pair structures are defined in negative resist (AR-N, ALLRESIST GmbH) by electron-beam lithography. Ion beam etching (Ar⁺ ions) of the gold layer is then carried out to generate the gold wire-pair structures. Subsequently, a 70-nm-thick spacer layer is applied on the first layer by spin-coating. A solidifiable photo polymer, PC403 (JCR), is used as the planarized spacer layer. A pre-baking process by continuously increasing the baking temperature from 90 to 130 °C is first carried out to remove the solvent from the polymer. A sufficiently long bake at a higher temperature (30 min in a 180 °C oven) further hardens the layer. A 40 nm gold film and a spin-coated AR-N resist layer are subsequently deposited on the sample. Next, the stacking alignment using the gold alignment marks is applied to ensure the accurate stacking of the second layer. Subsequently, the procedures of in-plane fabrication are repeated. The final layer is PC403. All structures have a total area of $200\,\mu m \times 200\,\mu m$.

Optical and structure characterization. Optical spectra are measured with a Fourier-transform infrared spectrometer (Bruker IFS 66v/S, tungsten lamp) combined with an infrared microscope (15 × Cassegrain objective, numerical aperture NA = 0.4, liquid-N₂-cooled MCT 77 K detector, infrared polarizer). The measured transmittance and reflectance spectra are normalized with respect to a bare glass substrate and a silver mirror, respectively.

The simulated field distribution is carried out by using the software package CST Microwave Studio. Optical parameters are the refractive index of PC403, $n_{PC403} = 1.55$ and the quartz substrate refractive index, $n_{glass} = 1.5$. The permittivity of bulk gold in the infrared spectral regime is described by the Drude model with plasma frequency $\omega_{pl} = 2\pi \times 2.175 \times 10^{15}\,s^{-1}$ and the damping constant $\omega_c = 2\pi \times 6.5 \times 10^{12}\,s^{-1}$. Owing to the surface scattering and grain boundary effects in the thin film of the real systems, the simulation result is obtained using a damping constant that is three times larger than the bulk value.

The electron micrographs of the fabricated structures are taken with a Hitachi S-4800 scanning electron microscope.

References

1. Boller, K. J., Imamoglu, A. & Harris, S. E. Observation of electromagnetically induced transparency. *Phys. Rev. Lett.* **66**, 2593–2596 (1991).
2. Harris, S. E. Electromagnetically induced transparency. *Phys. Today* **50**, 36–42 (1997).
3. Fleischhauer, M., Imamoglu, A. & Marangos, J. P. Electromagnetically induced transparency: Optics in coherent media. *Rev. Mod. Phys.* **77**, 633–673 (2005).
4. Hau, L. V., Harris, S. E., Dutton, Z. & Behrooz, C. H. Light speed reduction to 17 m s⁻¹ in an ultracold atomic gas. *Nature* **397**, 594–598 (1999).
5. Shvets, G. & Wurtele, J. S. Transparency of magnetized plasma at the cyclotron frequency. *Phys. Rev. Lett.* **89**, 115003 (2002).
6. Liu, C., Dutton, Z., Behrooz, C. H. & Hau, L. V. Observation of coherent optical information storage in an atomic medium using halted light pulses. *Nature* **409**, 490–493 (2001).
7. Lukin, M. D. & Imamoglu, A. Controlling photons using electromagnetically induced transparency. *Nature* **413**, 273–276 (2001).
8. Xu, Q. F. *et al.* Experimental realization of an on-chip all-optical analogue to electromagnetically induced transparency. *Phys. Rev. Lett.* **96**, 123901 (2006).
9. Alzar, C. L. G., Martinez, M. A. G. & Nussenzveig, P. Classical analog of electromagnetically induced transparency. *Am. J. Phys.* **70**, 37–41 (2002).
10. Waks, E. & Vuckovic, J. Dipole induced transparency in drop-filter cavity-waveguide systems. *Phys. Rev. Lett.* **96**, 153601 (2006).
11. Yanik, M. F., Suh, W., Wang, Z. & Fan, S. H. Stopping light in a waveguide with an all-optical analog of electromagnetically induced transparency. *Phys. Rev. Lett.* **93**, 233903 (2004).
12. Papasimakis, N., Fedotov, V. A. & Zheludev, N. I. Metamaterial analog of electromagnetically induced transparency. *Phys. Rev. Lett.* **101**, 253903 (2008).
13. Zhang, S., Genov, D. A., Wang, Y., Liu, M. & Zhang, X. Plasmon-induced transparency in metamaterials. *Phys. Rev. Lett.* **101**, 047401 (2008).
14. Verellen, N. *et al.* Fano resonances in individual coherent plasmonic nanocavities. *Nano Lett* **9**, 1663–1667 (2009).
15. Hao, F. *et al.* Symmetry breaking in plasmonic nanocavities: Subradiant LSPR sensing and a tunable Fano resonance. *Nano Lett.* **8**, 3983–3988 (2008).
16. Lal, S., Link, S. & Halas, N. J. Nano-optics from sensing to waveguiding. *Nature Photon.* **1**, 641–648 (2007).
17. Liu, N. *et al.* Three-dimensional photonic metamaterials at optical frequencies. *Nature Mater.* **7**, 31–37 (2008).
18. Tikhodeev, S. G., Yablonskii, A. L., Muljarov, E. A., Gippius, N. A. & Ishihara, T. Quasiguided modes and optical properties of photonic crystal slabs. *Phys. Rev. B* **66**, 045102 (2002).
19. Johnson, P. B. & Christy, R. W. Optical constants of the noble metals. *Phys. Rev. B* **6**, 4370–4379 (1972).
20. Ordal, M. A. *et al.* Optical properties of the metals Al, Co, Cu, Au, Fe, Pb, Ni, Pd, Pt, Ag, Ti, and W in the infrared and far infrared. *Appl. Opt.* **22**, 1099–1119 (1983).
21. Zhang, S. *et al.* Demonstration of metal-dielectric negative-index metamaterials with improved performance at optical frequencies. *J. Opt. Soc. Am. B* **23**, 434–438 (2006).
22. Dolling, G., Enkrich, C., Wegener, M., Soukoulis, C. M. & Linden, S. Simultaneous negative phase index and group velocity of light in a metamaterial. *Science* **312**, 892–894 (2006).
23. Prodan, E., Radloff, C., Halas, N. J. & Nordlander, P. A hybridization model for the plasmon response of complex nanostructures. *Science* **302**, 419–422 (2003).
24. Ropers, C. *et al.* Femtosecond light transmission and subradiant damping in plasmonic crystals. *Phys. Rev. Lett.* **94**, 113901 (2005).
25. Tassin, P., Zhang, L., Koschny, T., Economou, E. N. & Soukoulis, C. M. Low-loss metamaterials based on classical electromagnetically induced transparency. *Phys. Rev. Lett.* **102**, 053901 (2009).
26. Tassin, P., Zhang, L., Koschny, T., Economou, E. N. & Soukoulis, C. M. Planar designs for electromagnetically induced transparency in metamaterials. *Opt. Express* **17**, 5595–5605 (2009).
27. Liu, N., Liu, H., Zhu, S. N. & Giessen, H. Stereometamaterials. *Nature Photon.* **3**, 157–162 (2009).

Acknowledgements

Author contributions

All authors contributed extensively to the work presented in this paper.

Additional information